RSC Advances

PAPER

View Article Online
View Journal | View Issue

Check for updates

Cite this: *RSC Adv.*, 2017, **7**, 19725

Observation of local changes of "carbon-to-metal ratio" in the growth mechanism of carbon nanostructures grown from FePd-based and Fe_3C catalysts by pyrolysis of ferrocene and dichlorocyclooctadiene-palladium mixtures: the crucial role of Cl†

Filippo S. Boi, *[a] Zhang Xiaotian,[a] Sameera Ivaturi,[a] Yi He[b] and Shanling Wang*[b]

One of the major challenges in the field of carbon nanomaterials consists of understanding their growth mechanism dynamics. Recent reports have shown preliminary steady state chemical vapour deposition (CVD) experiments for the encapsulation of FePd-based alloys inside carbon-based nanostructures. However, very little is known about their growth mechanism dynamics. Here we investigate the possible presence of local changes of "carbon-to-metal ratio" in the growth mechanism of carbon nanostructures grown from FePd-based and Fe_3C catalyst-particles by steady state CVD and viscous-boundary-layer chemical vapour synthesis (CVS) experiments involving the pyrolysis of ferrocene/dichlorocyclooctadiene-palladium mixtures and of ferrocene/dichlorobenzene mixtures. In the first case, we demonstrate the observation of an unusual growth mechanism in which a direct transition from a spherically elongated carbon-onion-like (CNOs-like) morphology (low carbon-to-metal ratio condition) to a carbon fiber-like morphology (high carbon-to-metal ratio condition) is present within the same carbon structure. We attribute such transitions to the variation of the Cl-radicals concentration during the pyrolysis process, which implies a variation in the local "carbon to metal ratio" parameter. The reported mechanism is then compared in detail with that of Fe_3C filled CNTs obtained by CVD of ferrocene/dichlorobenzene mixtures and with those reported in the literature for other transition metal catalyst systems. In contrast, when a viscous boundary layer is created between the pyrolysed ferrocene/dichlorocyclooctadiene-palladium precursors and a rough surface, radial CNT structures filled with large quantities of both $FePd_3$ and Fe_3C crystals are found as major reaction products. The presence of filled-CNOs within the radial structures-core (resulting from the homogeneous nucleation of particles in the viscous boundary layer) suggests that fluctuations in the local "carbon-to-metal ratio" are also present in this type of mechanism. The morphological, cross-sectional and structural properties of the obtained carbon structures are analyzed in detail by SEM, TEM, STEM, HRTEM, ED and X-ray diffraction.

Received 27th January 2017
Accepted 28th March 2017

DOI: 10.1039/c7ra01207a

rsc.li/rsc-advances

Open Access Article. Published on 03 April 2017. Downloaded on 5/17/2026 12:24:15 AM.
This article is licensed under a Creative Commons Attribution-NonCommercial 3.0 Unported Licence.

Introduction

Since 1991, carbon nanotubes (CNTs) and carbon nano-onions (CNOs) have attracted great attention in the field of nanotechnology owing to their exceptional physical and chemical properties.[1–8] In particular great attention has been focused on the important chemical stability of these nanostructures which allows the encapsulation of specific materials (metals, semiconductors or alloys) of interest and their protection from oxidation.[6–16] Three main synthesis approaches of such nanostructures have been developed up to now: arc-discharge approaches,[6–8] solid state or liquid state chemical vapour deposition (SSCVD or LCVD)[9–16] and viscous boundary layer chemical vapour synthesis (BLCVS).[17–20]

Some of the most attractive materials encapsulated within CNTs and CNOs are single crystals of metals with ferromagnetic properties. In particular the encapsulation of single crystals of Fe_3C and FePd has attracted a great attention due to the exceptional anisotropy properties which are at the origin of the potentially giant coercivities achievable in these materials.[9–23] However despite the numerous reports in literature, the growth

[a]College of Physical Science and Technology, Sichuan University, Chengdu, China. E-mail: f.boi@scu.edu.cn

[b]Analytical and Testing Center, Sichuan University, Chengdu, China. E-mail: wangshanling@scu.edu.cn

† Electronic supplementary information (ESI) available. See DOI: 10.1039/c7ra01207a

Open Access Article. Published on 03 April 2017. Downloaded on 5/17/2026 12:24:15 AM.
This article is licensed under a Creative Commons Attribution-NonCommercial 3.0 Unported Licence.

mechanism of these nanostructures are not fully understood and require further investigations.

In particular, considering previous works on the encapsulation of metal-particles inside CNTs by arc-discharge processes,[6–8] the work by Elliott *et al.* had a great significance since it attempted to create a general qualitative carbon nanostructures growth map on the basis of the cumulative results in literature. This important growth map is based on two main growth parameters: the local-path carbon-to-metal ratio (LCM) and the global carbon-to-metal ratio (GCM). LCM refers to metal particles having the same local conditions along the same spatial pathway, while the GCM determines the weighting between different LCMs.[6] Considering the growth map of Elliott *et al.*[6] it is possible to assume that the formation of CNOs is favourable only with slow cooling rates and low carbon supply or in conditions where the diffusion carbon flux (diffusion toward the particle surface) is dominant. Therefore two types of carbon supply can be identified: type 1 expulsion (from the particle core to the external surface) and type 2 deposition (from the external surface to the particle core).[6] For slow growth processes the final product was found to depend on the difference between the particle–graphite interface energy and the vacuum surface energies γ, and the energy to bend the graphite sheets.[6] In particular the formation of CNOs has been associated to growth-conditions with low γ interaction.[6]

Thus, according with this map, a low value of (local) carbon to metal ratio results in a high metal nanoparticle count and consequently rapid consumption of carbon feedstock which tends to diffuse into the nucleated particles. As a consequence the formation of a metastable metal carbide can be expected. The decomposition of such carbide phase would then drive the flow of carbon within the particle core toward the particle-surface where the formation of graphitic layers will take place. The most likely product for this kind of growth conditions is therefore a metal nanocrystal encapsulated in a graphitic shell.[6] Differently a higher value of carbon to metal ratio would result in the formation of carbon nanotube structures due to the higher value of local carbon supply. The highest carbon to metal ratio regime will then result in the formation of urchin-like nanotube structures, induced by a fast nucleation process or spring like-structures and nanotube structures.[6] It seems therefore clear that the (local) carbon to metal ratio parameter controls the formation mechanism of single carbon-nanostructures products and that, following the reported map, no hybrid CNTs/CNOs structures have been yet observed.

Further reports of the growth mechanism and filling process of metal-filled CNTs structures were also given in 1999 by Demoncy *et al.* Indeed it was shown that the presence of sulfur in arc discharge methods has a key role in promoting the filling rates of numerous type of metals such as chromium, nickel and germanium within the CNTs core.[7,8] A nucleation and growth mechanism consisting of 4 main steps was suggested as follows: a first step involving the growth of CNTs from a carbon-rich metal particle deposited on the cathode. A second step in which sulfur promotes the carbon precipitation and is then trapped by the metallic material. A third step in which the S-enriched liquid will then flow inside the CNTs core and a fourth step involving the solidification of the metal-filling material.[7,8]

Recently CVD methods have largely replaced arc-production approaches for the achievement of single growth products. These methods can indeed guarantee LCM control by careful reactor design and careful control of process parameters.[9–16] However, in CVD processes the filling rate of the obtained carbon nanostructures is generally strongly dependent on the stoichiometry of the used metallocene precursor; thus the global carbon to metal ratio (GCM) is fixed by the stoichiometry of the used metallocene molecules (for steady state conditions). The results of these experiments generally yield CNTs partially filled with metal or interstitial-alloy particles, rather than long nanowires. Specifically in these experiments the nucleation and growth of the filled CNTs structures is generally described by a vapor liquid solid (VLS) mechanism as follows:[24–27]

(1) Exothermic catalytic decomposition of hydrocarbons at the surface of the transition metal–carbon nanoparticles at elevated temperature.

(2) The carbon species diffuse into the metal nanoparticle until the solubility limit is reached.

(3) A metastable carbide is formed.

(4) Due to carbide instability, the carbon precipitates on the particles surface and crystallizes into energetically stable graphitic carbon (endothermic process).

(5) Alternatively, a high carbon flux at the nanoparticle surface can also result in graphitic shell formation.

(6) The temperature gradient created by the exo- and endothermal processes would then drive the growth of the carbon nanostructure.

These growth-mechanism features are generally accepted for the description of CNTs growth. However several issues related to the control of the evaporation process of the used precursors still remain and can strongly limit the control of the LCM parameter. Indeed recent reports have shown that for CVD experiments performed in presence of dichlorobenzene/ferrocene mixtures[28–37] the presence of in-homogeneities in the pyrolysed metallocene vapour can lead to a variation in the morphology of the grown films in conditions of high pyrolysis temperatures.[28–31] The presence of such in-homogeneities has been attributed to the physical time-scale necessary for reaching the desired temperature of the preheater used for the precursor-evaporation. Within this time-scale, the inhomogeneous evaporation rate of the precursor (*i.e.* not all the grains of the metallocene reach the melting status simultaneously) will translate in a not homogeneous pyrolysed vapour. Furthermore, due to the presence of Cl radicals which spontaneously form CCl_4 species, the use of extremely low flow rates may change the carbon to metal ratio-value leading to the formation of an CNOs-product.[30] The presence of Cl radicals in a CVD reaction is therefore expected to change for a limited time the LCM parameter.

Interestingly, another type of synthesis method known as "viscous boundary layer chemical vapour synthesis" which has recently attracted important attention, tends to exploit local pathway fluctuations by deliberately creating a viscous boundary layer between a rough surface and a laminar

 This journal is © The Royal Society of Chemistry 2017

Open Access Article. Published on 03 April 2017. Downloaded on 5/17/2026 12:24:15 AM.
This article is licensed under a Creative Commons Attribution-NonCommercial 3.0 Unported Licence.

metallocene/Ar flow. Such viscous boundary layer has been reported to induce (1) the homogeneous nucleation of spherical metal particles in the pyrolysed metallocene vapour and (2) the subsequent growth of radial CNTs morphologies characterized by exceptional metal filling rates.[17–20] In addition, in these type of experiments the metallocene evaporation temperature has been reported to play a crucial role in selecting the growth of specific CNTs or CNOs morphologies.[20] So far these studies have been mainly performed for the specific case of Fe-, Ni- or Co-containing metallocenes.[17–20] Interestingly recent reports have shown preliminary steady state CVD experiments for the encapsulation of FePd-based alloys inside carbon-based nanostructures. However, very little is known about their growth mechanism dynamics.[21–23] Indeed the formation of unusual CNTs morphologies has been reported as result of low vapour flow-rate (steady state flow) pyrolysis of ferrocene/dichlorocyclooctadiene-palladium mixtures.

In this work we investigate in higher detail the growth mechanism of carbon nanostructures obtained by pyrolysis of Fe- and Pd-containing metallocene-like precursor in steady state CVD and viscous boundary layer CVS methods. In particular we report the observation of an unusual growth mechanism in which a direct transition from a CNOs morphology to a carbon fiber-like morphology is observed within the same carbon structure. This is found in conditions of low vapour flow-rate (steady state flow) CVD involving pyrolysis of ferrocene/dichlorocyclooctadiene-palladium mixtures. The cross sectional morphology, structure and growth mechanism of the obtained structures are investigated in detail by transmission electron microscopy (TEM), high resolution TEM (HRTEM) and electron diffraction (ED). The observed growth mechanism is then compared with of Fe_3C filled CNTs produced by CVD of ferrocene/dichlorobenzene mixtures. In contrast, for experiments performed in the presence of a viscous boundary layer between the pyrolysed metallocene-like precursors and the used rough surface of the substrate, radial CNTs structures filled with $FePd_3$ and Fe_3C crystals are found as major product in the reaction. This latter result confirms the existence of the radial structure growth mechanism also in presence of Fe and Pd species. However much lower filling rates with respect to those previously observed by Boi *et al.* in the case of single ferrocene or mixed metallocenes-pyrolysis are found due to the low solubility of carbon in $FePd_3$ alloys. The morphological, cross-sectional and structural properties of the obtained radial structure are analyzed in detail by SEM, TEM, scanning TEM (STEM), HRTEM and X-ray diffraction.

Experimental

The used CVD/CVS system consisted of one pre-heater zone, one reaction zone and a quartz tube reactor. The pre-heater and reaction zone furnaces are mounted in a rail-system. This allows to perform a fast cooling (quench) by sliding the reaction zone furnace along the rail system after each reaction. Note that two methods of precursor evaporation have been used. In the method-1, the precursors are placed in proximity of the substrate used for the product-deposition and evaporated after sliding the main-reaction zone furnace along the rail system (see ESI Fig. 1†). This allows a fast evaporation process.

Instead in the method-2 (ESI Fig. 2†) the reactants are evaporated from the preheater-zone. Due to the very low evaporation temperature used in some of the experiments, an inhomogeneous evaporation rate of the precursor (*i.e.* not all the grains of ferrocene reach the melting status simultaneously) is expected. Two schematics of the used CVD reactors can be found in ESI Fig. 1 and 2.† See Fig. 3 and 4† ESI for table showing the molar ratios of the used reactants. The following experimental conditions were used:

Hybrid CNO/CNF-like structures: 90 mg of dichlorocyclooctadiene-palladium (0.00032 mol) and 90 mg of ferrocene (0.00048 mol) were evaporated at 300 °C (method-1) and pyrolyzed at 1050 °C (molar ratio of the reactants: 1.53475). An Ar flow rate of 10–12 ml min^{-1} was used. The used quartz tube reactor consisted of the following dimensions: a quartz tube with a length of 1.5 m, an outer diameter of 22 mm and a wall thickness of 2.5 mm. Note that in this type of experiments no preheater was used; instead the reactants were placed in proximity of a Si/SiO_2 (111) substrate used for the product-deposition at a distance of approximately 3 cm. The reaction time was of approximately 10 min.

Fe_3C filled CNTs type 1 : 0.05 ml of dichlorobenzene (0.00042 mol) and 60 mg of ferrocene (0.00032 mol) were evaporated at 300–350 °C (method-1) and pyrolysed at 990 °C (molar ratio of the reactants: 0.76010). An Ar flow rate of 10–12 ml min^{-1} was used. The used quartz tube reactor consisted of the following dimensions: a quartz tube with a length of 1.5 m, an outer diameter of 22 mm and a wall thickness of 2.5 mm. A Si/SiO_2 substrate (111) was placed in the reaction zone for the deposition of the growth product. The reaction time was of approximately 10 min. Note that in this type of experiments no preheater was used; instead the reactants were placed in proximity of a Si/SiO_2 substrate used for the product-deposition at a distance of approximately 3 cm. In this region of the reactor a temperature of 300–350 °C was measured with a thermocouple.

Fe_3C filled CNTs type 2 : 0.15 ml of dichlorobenzene (0.00127 mol) and 1.5 g of ferrocene (0.00806 mol) were evaporated at 70 °C (method-2) and pyrolysed at 990 °C (molar ratio of the reactants: 6.33423). An Ar flow rate of 5 ml min^{-1} was used. The reaction time was of 1 h. The used quartz tube reactor consisted of the following dimensions: a quartz tube with a length of 1.5 m, an inner diameter of 44 mm and a wall thickness of 3 mm. A Si/SiO_2 substrate (111) was placed in the reaction zone for the deposition of the growth product.

Radial CNTs structures filed with $FePd_3$: 1.1 g of ferrocene (0.00591 mol) and 0.3 g of dichlorocyclooctadiene-palladium (0.00105 mol) were evaporated at the temperature of approximately 200 °C (method-2) and pyrolysed at the temperature of 990 °C (molar ratio of the reactants: 5.62742). An Ar flow rate of 11 ml min^{-1} was used. The reaction time was of 1 h. The used quartz tube reactor consisted of the following dimensions: a quartz tube with a length of 1.5 m, an inner diameter of 44 mm and a wall thickness of 3 mm. In this latter case the radial structures are grown in the viscous boundary layer created by introducing a rough surface (roughness in the order of 100

Open Access Article. Published on 03 April 2017. Downloaded on 5/17/2026 12:24:15 AM.
This article is licensed under a Creative Commons Attribution-NonCommercial 3.0 Unported Licence.

micrometres) in the deposition zone of the reactor. A disappearance of the radial structure morphology was observed when high evaporation temperatures of approximately 350–500 °C were used. Instead relatively low evaporation temperatures favoured the formation of the radial structures.

The characterization and growth mechanism investigation was performed with the following technique: TEM, HRTEM, (selective area) ED (SAED) with a 200 kV American FEI Tecnai G^2F20. For these analyses the as grown structures were first dispersed in samples bottles with ethanol. The TEM samples were then prepared by depositing a small quantity of the as dispersed material on the top of a TEM grid comprising a holey carbon film and a copper grid-frame. Note that no ultrasonication method was used for the dispersion. SEM analyses were performed with a JSM-7500F at 5–20 kV. XRD analyses were performed with an Empyrean Panalytical diffractometer (Cu K-α with $\lambda = 0.154$ nm). The characterization of the raw data extracted from the as measured XRD pattern was then performed by conversion of the .xrdml files into a .gsa format for Rietveld refinement analyses. The Rietveld method, which uses the least-squares approach to match a theoretical line profile to the diffractogram, was used to identify and estimate the relative abundances of the encapsulated phases from the area enclosed by the diffraction peaks. This method allowed also for the extraction of the unit-cell parameters of the crystal phases encapsulated inside the grown carbon nanostructures.

Results and discussion

The morphology of the unusual carbon structures obtained with the first approach was firstly revealed by SEM micrographs. As shown in Fig. 1 these fiber-like structures (CNFs) exhibit an unusual urchin-like morphology and appear to grow in all the areas of the substrate. In particular Fig. 1A shows the morphology of these structures from a top view, while Fig. 1B shows the morphology with a higher detail. Further cross-sectional analyses were then considered with the use of TEM.

As shown in Fig. 2A these analyses revealed the presence of a cross-sectional morphology characterized by two main regions. A base region comprising unusual elongated approximately spherical CNOs-like particles which can be hollow or can encapsulate FePd-based alloys (see red arrow), and an intermediate region with a fiber-like structure which terminates with a capping-like closure (see inset). The observation of a direct transition from an CNOs-like morphology into a fiber-like morphology (CNF) is very unusual and to the best of our knowledge has not been reported in previous literature reports. Note that, as shown in Fig. 2A with the magenta arrow and in Fig. 2B with an higher detail the transition from an CNOs-like morphology into a CNF-like morphology appears to be linked to a change of shape of the CNOs-like particles shells and volume. This observation is also confirmed by TEM micrographs of the transition area taken with a higher detail (see magenta arrow in Fig. 2C).

Considering the growth mechanism of carbon nanostructures described in the qualitative map of Elliott *et al.*,[6] it is possible to notice that none of the described morphologies has

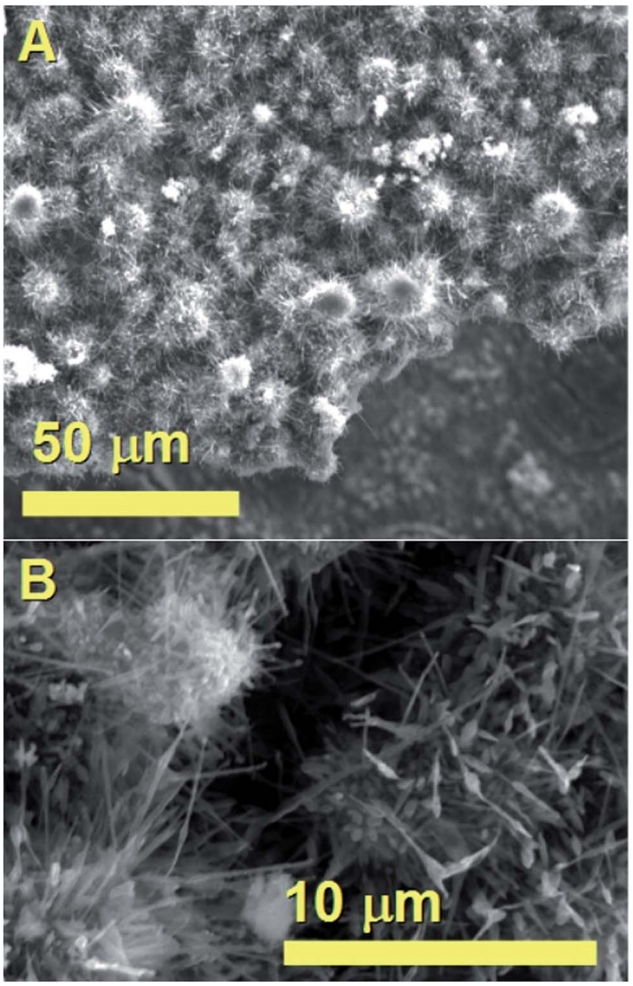

Fig. 1 SEM micrographs showing in (A) and (B) the urchin-like morphology of the as grown hybrid CNO/CNF structures.

similarity with that shown in Fig. 2. The formation of CNOs- and CNTs-like structures require in principle different values of LCM. Indeed the CNOs morphology requires low values of local carbon to metal ratio, while elongated CNTs-like structures require high values of local carbon to metal ratio. The growth of the hybrid structure in Fig. 2 could be therefore explained by considering the presence of a local variation in the carbon to metal ratio parameter during the growth.

Such variation could be associated to the variation of Cl-concentration in the pyrolysed vapour, which is expected to remove carbon-species by forming chlorinated carbon clusters (CCl_4).[30–37] In order to verify this interpretation further experiments were performed by using ferrocene and dichlorobenzene as precursors with experimental conditions similar to those reported by Boi *et al.* and Guo *et al.*[28,30] Interestingly, as shown in Fig. 3 (see Experimental section, for Fe_3C filled CNTs type 1, method-1 of evaporation) the two types of morphologies, namely fully filled CNTs and filled CNOs-like structures could be observed.

However, differently with respect to the hybrid-nanostructure shown in Fig. 1 and 2, in this case the CNTs and CNOs-like structures are found in the form of separate

 This journal is © The Royal Society of Chemistry 2017

Open Access Article. Published on 03 April 2017. Downloaded on 5/17/2026 12:24:15 AM.
This article is licensed under a Creative Commons Attribution-NonCommercial 3.0 Unported Licence.

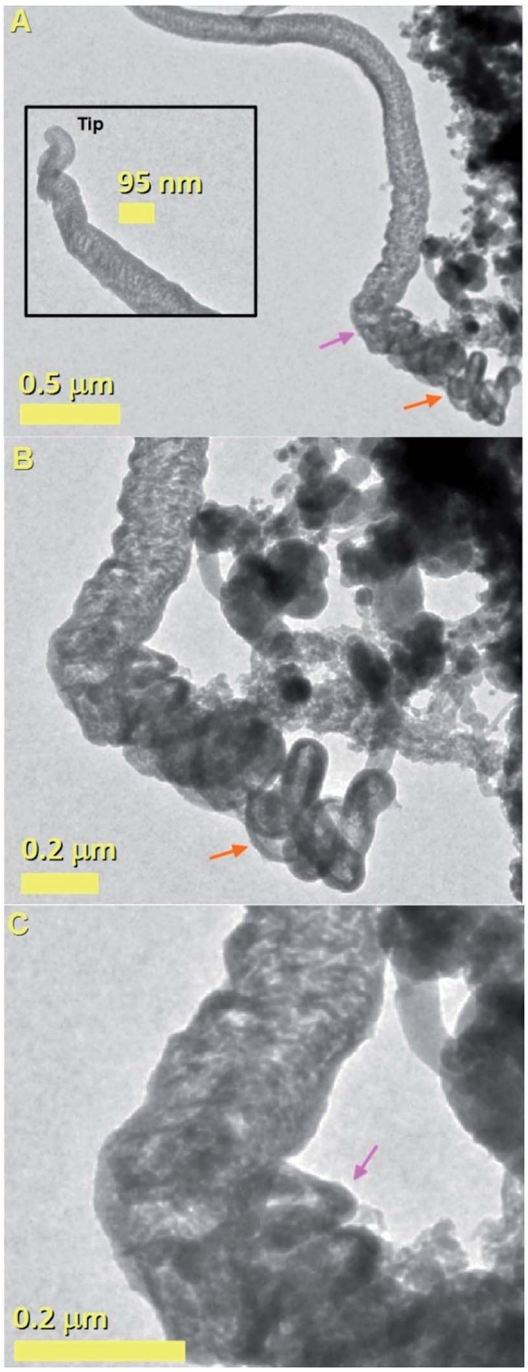

Fig. 2 TEM micrographs showing the morphology of a typical unusual CNOs/CNF hybrid carbon nanostructure with an increasing level of detail. A transition from a CNO-morphology (see red arrow in A and B) into a CNF-like morphology is found in (C) (magenta arrow).

morphologies, with the CNOs-like structures being a minority by-product of the reaction (see also ESI Fig. 5†). See also ESI Fig. 6† for another TEM example of these structures. The carbon nanostructures shown in Fig. 3 are found to be filled with single crystal phase of Fe_3C with space group *Pnma*.

This interpretation is confirmed by the HRTEM analyses in Fig. 3B and C which show the presence of a preferred orientation

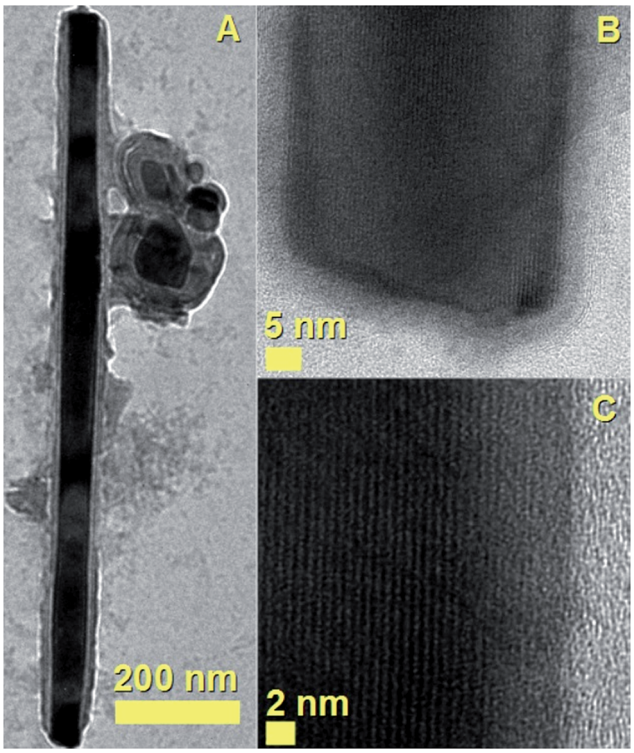

Fig. 3 TEM and HRTEM micrographs showing the morphology of a single crystalline Fe_3C nanowire encapsulated inside a CNTs with an increasing level of detail in (A)–(C). This nanostructure is obtained by pyrolysis of ferrocene (60 mg)/dichlorobenzene (0.05 ml) mixtures. In (A) the presence CNOs-like structures filled with Fe_3C particles is also observed.

of the encapsulated Fe_3C crystal with the 010 axis of the crystal pointing perpendicularly with respect to the CNT-walls.

This interpretation is confirmed also by Fourier transform investigation of the filled CNT, as shown in Fig. 4, which reveal the preferred crystal growth with direction perpendicular to the 010 crystal axis. The observed reflections are indexed as follows: the cyan circles correspond to the 010 reflection of Fe_3C (lattice spacing of 0.67 nm) while the magenta circles correspond to the 121 reflection of Fe_3C (lattice spacing of 0.24 nm). The observation of both CNTs and CNOs products could be considered also in this case a consequence of the presence of Cl-radicals in the CVD system. The formation of CNOs is indeed expected only in the first stages of precursor pyrolysis, when a very high concentration of Cl-species is present due to the high evaporation temperature of the precursors and a low carbon-to-metal ratio is probable. The carbon-to-metal ratio is then expected to change again once the Cl-radicals are consumed by the formation of CCl_4 species.

In order to confirm the interpretation above, further experiments were then considered in conditions of higher dichlorobenzene quantities of 0.15 ml, very low evaporation temperature of 70 °C and very low vapour flow rates of 5 ml min^{-1} (see Experimental section, for Fe_3C filled CNTs type 2, method-2 of evaporation). Indeed previous reports have shown that in these experimental conditions a crust of onions is present on the top

Open Access Article. Published on 03 April 2017. Downloaded on 5/17/2026 12:24:15 AM.
This article is licensed under a Creative Commons Attribution-NonCommercial 3.0 Unported Licence.

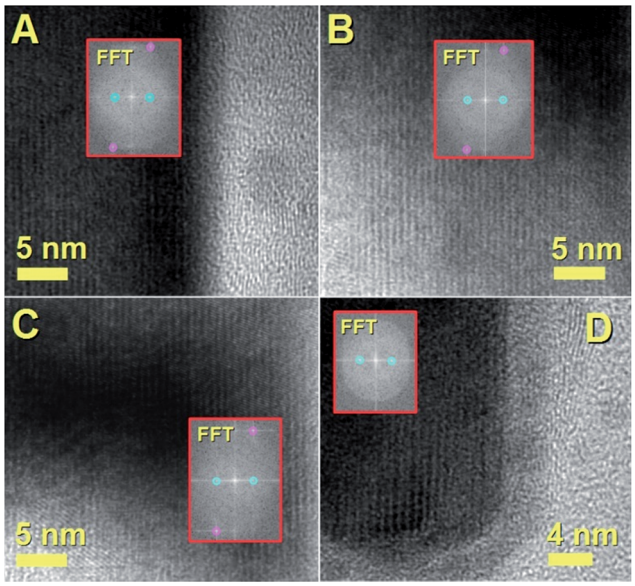

Fig. 4 HRTEM and FFT analyses of the single crystalline Fe_3C nanowire previously shown in Fig. 3.

of the obtained CNTs films.[30] In agreement with the observations reported in literature, we also find that in these experimental conditions a crust of CNOs is present on the top of the grown CNTs buckypaper-film (see Fig. 5 and 6 for SEM and TEM images of the CNOs crust).

The observation of such large quantity of CNOs can be associated to the presence of a low carbon to metal ratio conditions in the first stages of the CVD reaction, due to the presence of high quantities of Cl-radicals and low quantities of ferrocene. However, note that due to the low evaporation temperature used in this type of experimental conditions, the presence of Cl radicals is expected for timescales much longer.

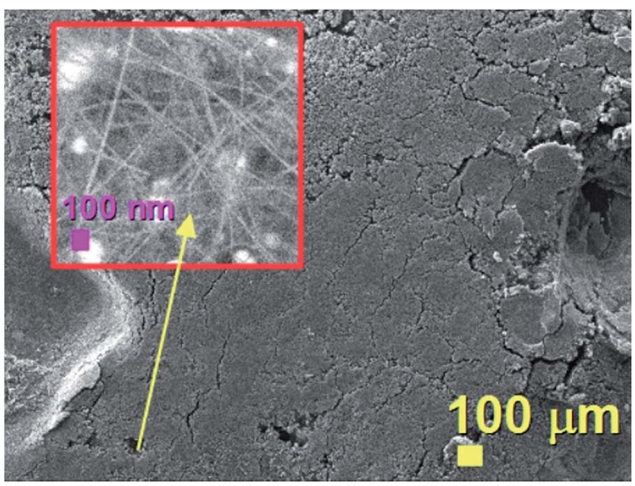

Fig. 5 SEM micrograph showing the morphology of the CNOs crust observed on the top of as grown CNTs-buckypapers (Fe_3C filled CNTs type 2, see Experimental section) produced by pyrolysis of ferrocene (1.5 g)/dichlorobenzene (0.15 ml) mixtures. The approximately-spherical bright areas in the inset correspond to the filled CNOs structures.

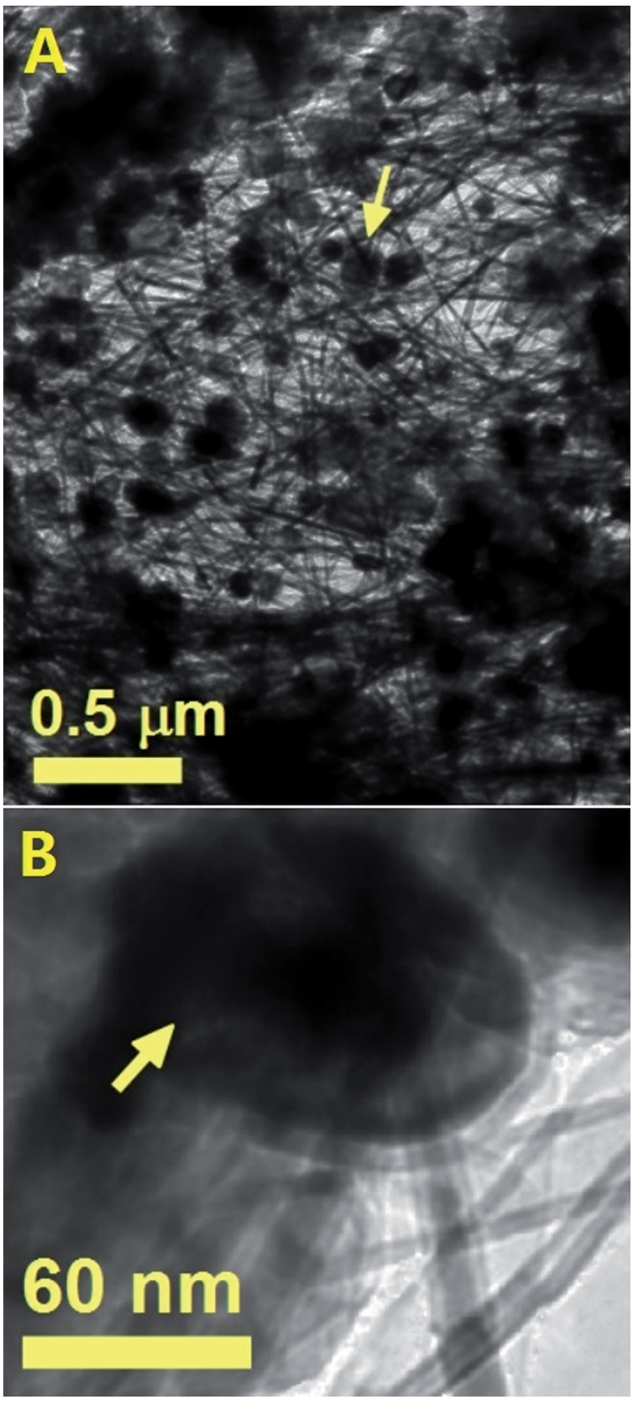

Fig. 6 TEM images (A and B) showing the morphology of the CNTs and CNOs (yellow arrow) previously shown with SEM micrographs in Fig. 5 and inset. In (B) a high detail of a CNO-structure comprised in the onion crust is shown.

These observations can justify the variation in the quantity of obtained CNOs with the evaporation temperature and Cl concentration in the vapour. Also, it is important to notice that in both these type of experiments, the observed carbon nanostructures are found in a separate morphology and don't form any hybrid structure.

 This journal is © The Royal Society of Chemistry 2017

Open Access Article. Published on 03 April 2017. Downloaded on 5/17/2026 12:24:15 AM.
This article is licensed under a Creative Commons Attribution-NonCommercial 3.0 Unported Licence.

These findings appear therefore to suggest two important key factors which can control the (local) carbon-to-metal ratio parameter described by Elliott *et al.*:[6] (i) the concentration of Cl-containing precursor which controls the concentration of Cl radicals in the pyrolysed vapour and (ii) the used catalyst (and therefore the variation of C-solubility parameters for the chosen catalyst[22]).[38–43] Indeed for the specific case of Fe_3C, the morphologies of the obtained nanostructures is comparable to those described in the map of Elliott *et al.*[6] Instead such comparison is not valid for the FePd-based catalyst case. This difference can be attributed also to the different carbon solubility in the two types of catalysts. In view of these observations, further analyses of the hybrid structures produced with FePd-based catalysts were considered.

Additional examples of the cross-sectional morphologies of the unusual CNFs structures shown in Fig. 2 are shown in Fig. 7–10. In Fig. 7A–C the CNOs-like structures observed in the base of the analysed CNFs are shown with increasing level of detail. Note that the majority of the CNOs structures are found to be catalyst-free and arranged with a surprising close-packing structure and a wide diameter of approximately 350–400 nm. A high detail of a CNOs-like structure filled with a FePd-based crystal is also shown in Fig. 7C (dark region). Another example of these type of nanostructures is shown in Fig. 8. Interestingly, as shown in Fig. 8A and B by the red and cyan arrow also in this case the presence of closepacked CNOs-like particles at the base of the CNF-structure were found. Examples of filled CNOs are also indicated with the magenta arrow in Fig. 8B. The lattice spacing observed in the CNOs shell structure is instead shown in Fig. 8C. The Fourier transform in the inset clearly shows the presence of a 002 reflection from graphitic carbon. A similar nanostructure is also shown in Fig. 9A and B. Also in this case the observed CNOs-like structures were found to be filled and unfilled. The HRTEM investigations confirmed not only the presence of a graphitic like arrangement of the CNOs shells, but also the presence of lattice spacing compatible with those of a $FePd_3$ phase (Fig. 9C). Such observation is also confirmed by further selective area ED analyses, as shown in Fig. 9D. Indeed ED measurements revealed the presence of a 002 graphitic reflection (blue arrow) corresponding to a lattice spacing of 0.356 nm and the presence of a lattice spacing of 0.197 nm which can be associated to the 200 reflections of $FePd_3$ with space group $Fm\bar{3}m$.

Further examples of these types of structures are also shown in Fig. 10. The red arrows in Fig. 10B and C indicate the CNOs-like particles at the base of the CNF. The morphology of the CNF is shown with a high detail in Fig. 10D.

From the analyses above, it seems therefore clear that the FePd-based catalyst-system leads to different reaction dynamics and does not follow directly the growth mechanism predicted by Elliott *et al.*[6] In addition, the observed morphology is much different with respect to that reported in recent reports on the encapsulation of $FePd_3$ crystals inside CNTs.[21] Such difference can be associated to the different carbon solubility (very low if compared to that in Fe) present in the $FePd_3$ phase and to the different quantity of dichloro-cyclooctadiene palladium employed in the reactions and therefore to the different concentration of Cl radicals.[21] Indeed the graphite-like morphologies reported recently by Boi *et al.* are obtained in conditions of much higher concentrations of Cl-containing precursor.[21] This implies the presence of a very low LCM which again can not be explained by the qualitative map reported by Elliott *et al.*, where graphite is expected at high LCM values.

In order to further investigate the properties of this system, additional experiments on carbon nanostructures grown from

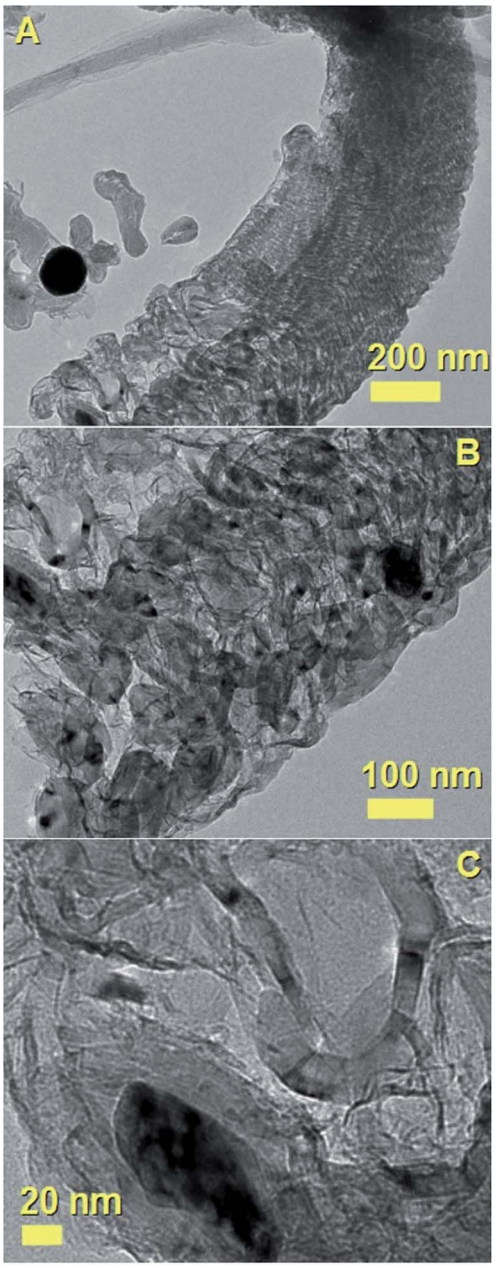

Fig. 7 TEM micrographs (A–C) showing another example of the unusual carbon nanostructures obtained by pyrolysis of 90 mg of ferrocene and 90 mg of dichlorocyclooctadiene-palladium. Also in this case the base region is found to comprise empty and filled CNOs with a closepacked arrangement. A high detail of the CNOs is shown in (B) and (C). Note that the diameter of this nanostructure is larger with respect to that shown in Fig. 2.

Open Access Article. Published on 03 April 2017. Downloaded on 5/17/2026 12:24:15 AM.
This article is licensed under a Creative Commons Attribution-NonCommercial 3.0 Unported Licence.

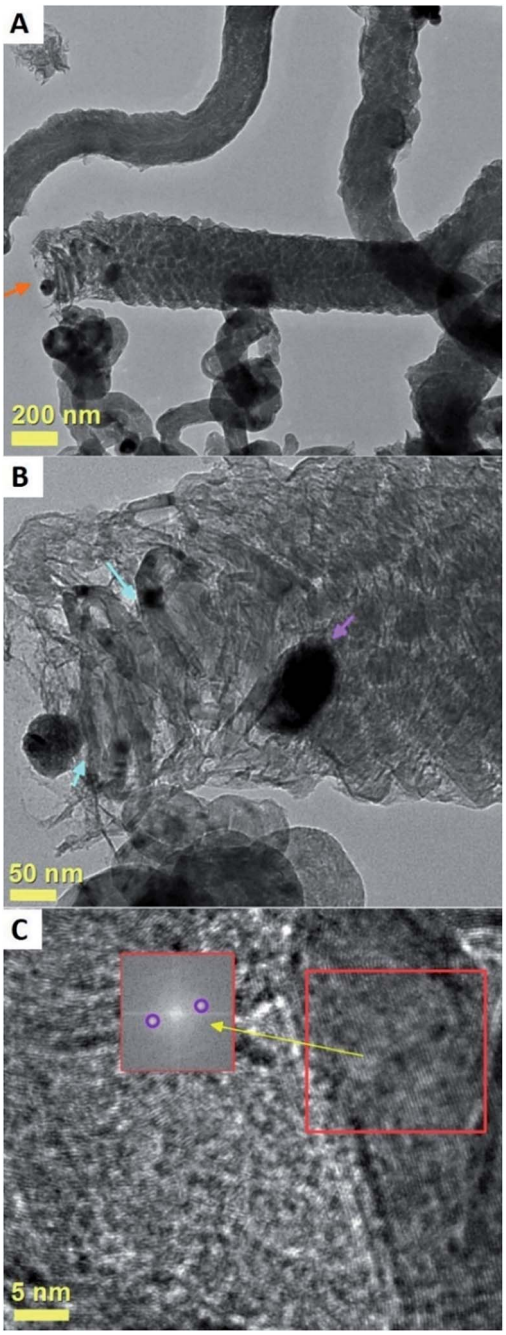

Fig. 8 TEM micrographs (A–C) showing further examples of unusual carbon nanostructures obtained by pyrolysis of 90 mg of ferrocene and 90 mg of dichlorocyclooctadiene-palladium. The base region is found to comprise empty (cyan arrow) and filled (magenta arrow) CNOs-like structures with a close-packed arrangement. A high detail of the CNOs-graphitic arrangement (analysed by Fourier transform of the lattice) is shown in (C). Note that the diameter of this CNF-like structure is in the order of 200 nm.

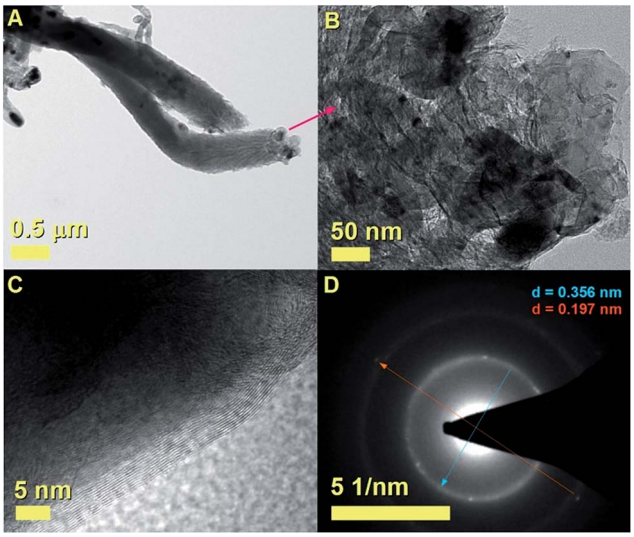

Fig. 9 TEM micrographs (A–C) showing more examples of the unusual CNFs obtained by pyrolysis of 90 mg of ferrocene and 90 mg of dichlorocyclooctadiene-palladium. The base region in (B) is found to comprise empty and filled CNOs-like structure with a closepacked arrangement. A high detail of the CNOs is shown in (C). In (D) the electron diffraction pattern of the area in (C) shows the 002 reflection of graphitic carbon and the 200 reflection of $FePd_3$.

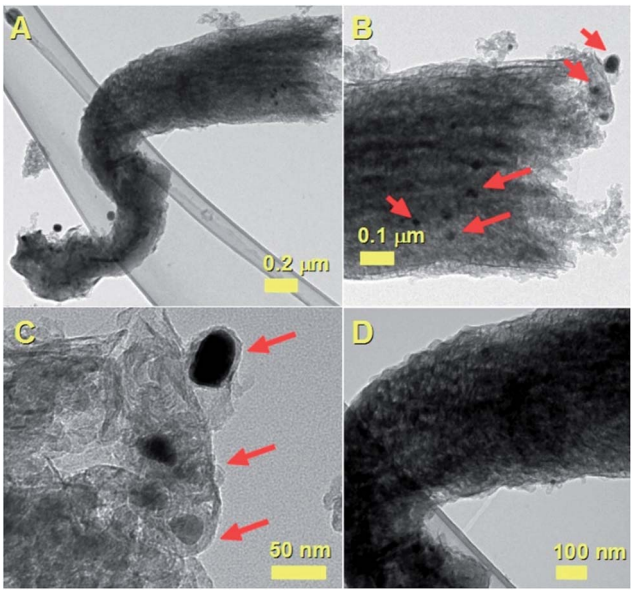

Fig. 10 TEM micrographs (A–D) showing the cross-sectional morphology of the carbon nanofiber (CNF)-like structure. In (B) and (C) a high detail of the CNOs-like particles at the CNF-base are shown.

FePd-based catalyst alloys were considered in presence of a viscous boundary layer. As mentioned above, viscous boundary layer CVS is a novel technique which allows (for the specific case of Fe-based catalyst) the growth of radial CNTs structures with exceptional filling rates by creating fluctuations in the (local) carbon to metal ratio. Up to now this technique has been used for the fabrication of radial structures filled with α-Fe, Fe_3C, γ-Fe, FeNi and FeCo.[17–20]

However no reports have demonstrated up to now the dynamics of the viscous boundary layer in presence of an iron- and palladium-rich pyrolysed vapour.

This journal is © The Royal Society of Chemistry 2017

Open Access Article. Published on 03 April 2017. Downloaded on 5/17/2026 12:24:15 AM.
This article is licensed under a Creative Commons Attribution-NonCommercial 3.0 Unported Licence.

The result of these experiments is shown in the SEM analyses of Fig. 11 and 12 and in the TEM analyses of Fig. 13. Interestingly, these measurements revealed that in presence of dichloro-cyclooctadiene-palladium as precursor together with ferrocene, radial CNTs structures are still obtained as dominant product of the reaction. Such experimental results can be associated to the much lower dichloro-cyclooctadiene-palladium concentrations (ferrocene/dichloro-cyclooctadiene-palladium molar ratio = 5.62742) which is fixed by both the precursor quantity and evaporation temperature and implies a relatively low concentration of Cl-radicals in the CVS system. Indeed high concentration of Cl are expected to inhibit the homogeneous nucleation mechanism of CNOs and therefore prevent the growth of radial structures. Note that a complete disappearance of the radial structure morphology was found in conditions of very high evaporation temperatures of the dichloro-cyclooctadiene-palladium (approximately 350–500 °C) precursor due to the much higher Cl-concentrations achievable in those conditions. As shown in Fig. 13A by the red arrows and in Fig. 13B in scanning TEM mode, the radial structures obtained in conditions of low evaporation temperature (approximately 200 °C) are characterized by a core constituted by an agglomeration of CNOs. These characteristics can be clearly visualized in Fig. 13B in STEM mode, thanks to the atomic contrast (bright areas). This result is in agreement with those reported in previous literature reports on viscous boundary layer created by rough surfaces, where the obtained product consisted of radial structures filled with ferromagnetic α-Fe, Fe_3C, FeNi or FeCo and characterized by an agglomeration of CNOs as central core.[17–20] The CNTs growing from the radial structure core are shown in Fig. 13C and 14 (magenta arrow). Note that the CNTs are found to grow with a high alignment. A higher detail of the central core of the radial structures previously show in Fig. 13A and B is also shown in Fig. 14. The orange arrow indicates a typical high-magnification example of CNO comprised in the radial structure core.

An example of aligned CNTs grown from the radial structure is then shown in Fig. 15. Note that the aligned CNTs exhibit a small diameter in the order of 50 nm. An example of FePd based particle encapsulated within the CNT core is indicated by the red star in Fig. 15. Owing to the high thickness of the radial structures, HRTEM or ED analyses could not be successfully performed in these structures. Further evidence of the structural arrangement of the encapsulated FePd-based phases was then sought by XRD.

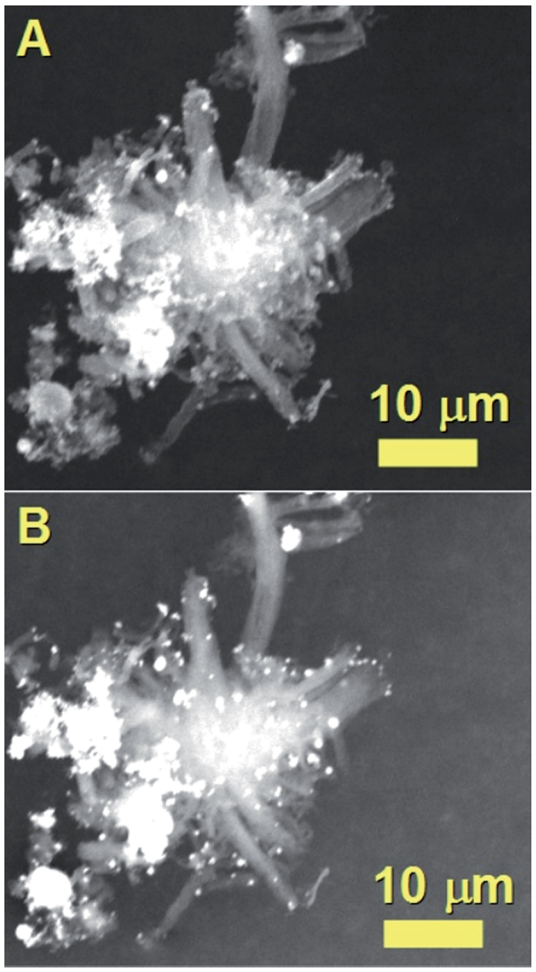

Fig. 12 SEM micrograph showing the morphology of a typical as grown radial structure with secondary electrons in (A) and backscattered electrons in (B). Backscattered electrons are sensitive to the variation in atomic number and can be used to clearly visualize the radial structure core.

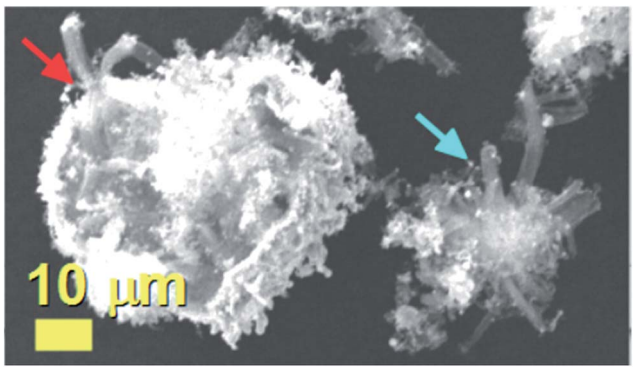

Fig. 11 SEM micrographs showing the morphology of the as grown radial CNTs-structures filled with $FePd_3$. As shown by the red arrow these structures are found to be clustered-together in large clusters. The cyan arrow indicates an example of isolated radial structure.

A typical XRD pattern of the as grown powder containing radial structures is shown in Fig. 16. Interestingly, in agreement with previous experiments performed with the only ferrocene,[17] also in this case two main carbon peaks could be found in the region of 26 degrees 2θ. The first peak indicated with the magenta star is associated to the contribution of the graphitic walls of the CNTs comprised in the radial structures (002 reflection). Instead the second peak indicated with the red star could be assigned to the contribution of the graphitic carbon in the CNOs comprised in the radial structures core. Further analyses at higher values of 2θ degrees revealed the presence of several metal and alloys phases within the sample. Note that the presence of FePd-based ($FePd_3$) phases was confirmed by the

Open Access Article. Published on 03 April 2017. Downloaded on 5/17/2026 12:24:15 AM.
This article is licensed under a Creative Commons Attribution-NonCommercial 3.0 Unported Licence.

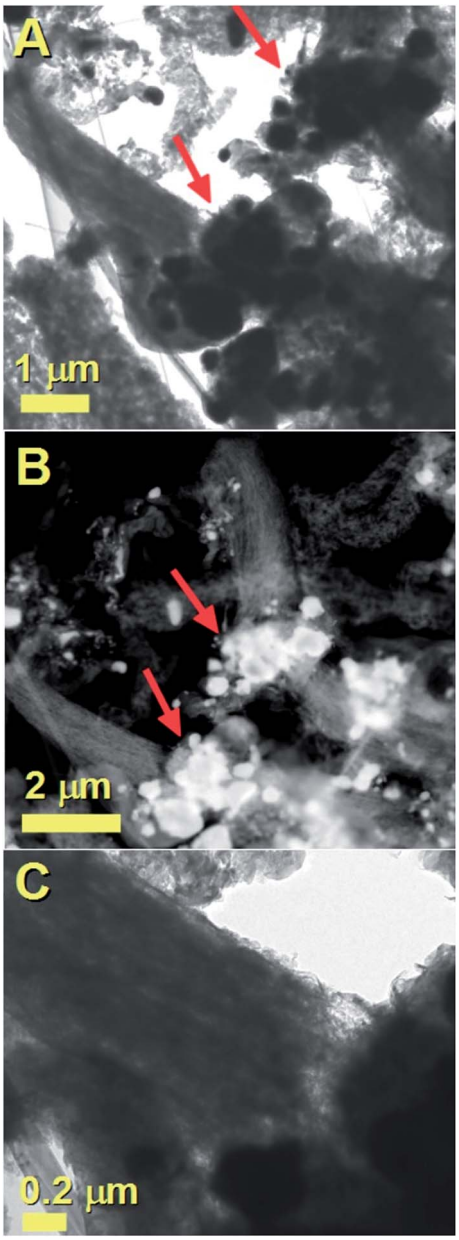

Fig. 13 TEM micrographs showing the morphology of the radial structures obtained by pyrolysis of 1.1 g of ferrocene and 0.3 g of dichlorocyclooctadiene-palladium in presence of a viscous boundary layer created between the rough substrate surface and the used laminar Ar flow. In (A) the TEM micrograph shows two typical radial structures (see red arrows). The CNOs core-agglomeration in the radial structure core can be clearly visualized with STEM analyses (bright regions) in (B). In (C) a high detail of the aligned filled CNTs departing from the central core is shown.

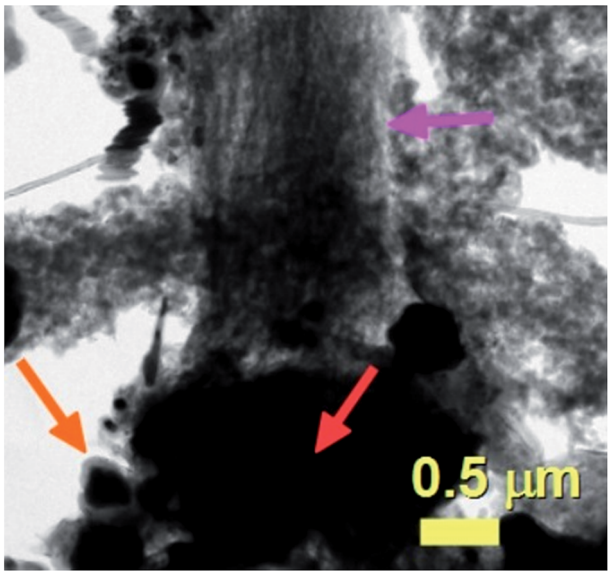

Fig. 14 TEM micrograph showing a high detail of one of the radial structures shown in Fig. 9. The red arrow indicates the central core of the radial structure. Due to the high thickness of the central core the CNOs can be visualized only in relatively thin part of the core as shown by the orange arrow.

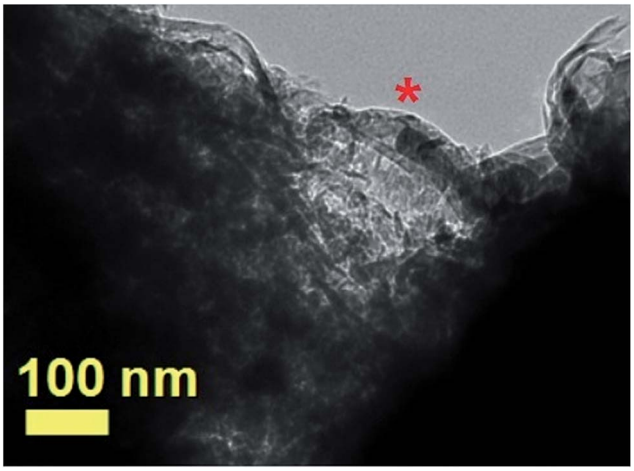

Fig. 15 TEM micrograph showing with a high detail the CNTs departing from a radial-structure core. A typical CNT filled with a FePd-based alloy is indicated by the red star.

111 and 200 reflections of $FePd_3$ with space group $Fm\bar{3}m$. In addition other Fe-based phases such as Fe_3C, γ-Fe and α-Fe were found. Further confirmation of this interpretation was sought by Rietveld refinement analyses. Interestingly, as shown in Fig. 17 these analyses confirmed the interpretation above and allowed for the extraction of the following metal/alloy phase abundances: 24.3% of $FePd_3$ (unit cell parameters of $a = b = c$: 0.385 nm and $a = b = c$: 0.381 nm), 46.1% of Fe_3C with space group *Pnma* (unit cell parameters *a*: 0.510 nm, *b*: 0.675 nm, *c*: 0.453 nm), 17.8% of α-Fe with space group $Im\bar{3}m$ (unit cell parameters of $a = b = c$: 0.287 nm) and 11.8% of γ-Fe with space group $Fm\bar{3}m$ (unit cell parameters $a = b = c$: 0.360 nm). In particular the observation of two types of unit cell parameters for the specific case of $FePd_3$ suggests a possible role of the pressure imposed by CNTs or CNOs walls on the encapsulated crystals.

These analyses were further confirmed by the observation of a remarkable difference between the cross-sectional

This journal is © The Royal Society of Chemistry 2017

Open Access Article. Published on 03 April 2017. Downloaded on 5/17/2026 12:24:15 AM.
This article is licensed under a Creative Commons Attribution-NonCommercial 3.0 Unported Licence.

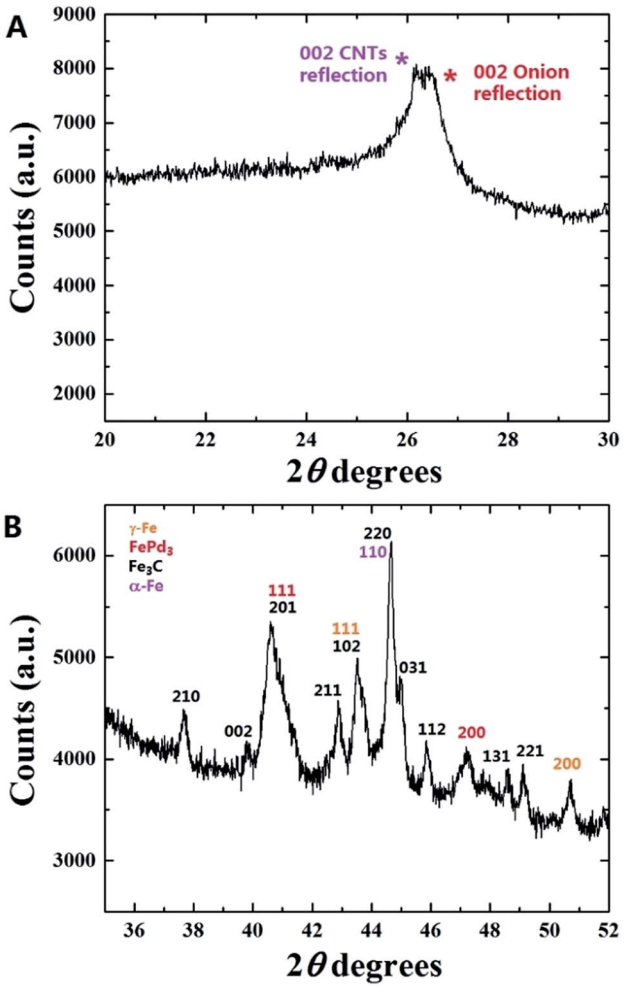

Fig. 16 XRD pattern in (A) and (B) of the as grown radial structure sample produced by pyrolysis of 1.1 g of ferrocene and 0.3 g of dichlorocyclooctadiene-palladium in presence of a viscous boundary layer created between the rough substrate surface and the used laminar Ar flow.

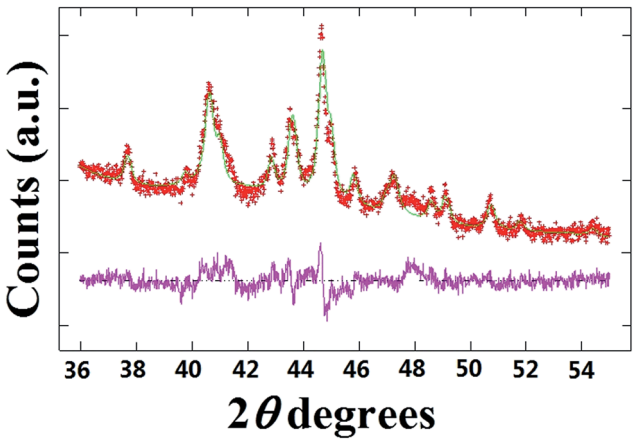

Fig. 17 Rietveld refinement of the XRD pattern shown in Fig. 16.

morphology of the CNTs encapsulating Fe-based crystals and the morphology of the CNTs filled with FePd-based phases. A typical example of Fe-filled CNT is shown in Fig. 18. Note that in this case a much larger diameter and a high CNTs-wall thickness is found.

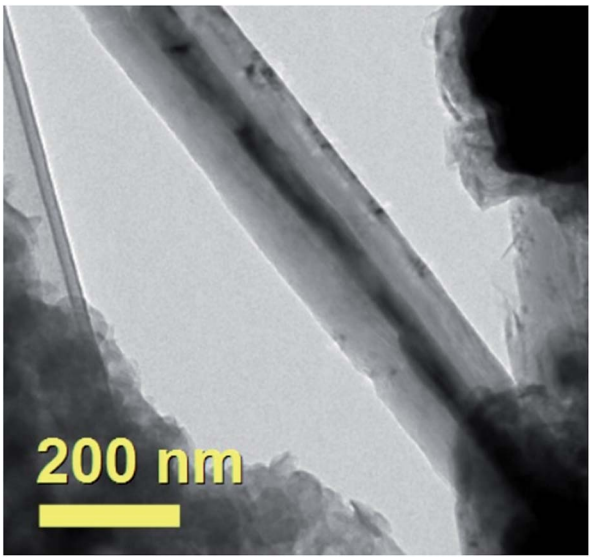

Fig. 18 TEM micrograph showing the typical morphology of a Fe-filled CNT comprised in the as grown radial structure sample shown in Fig. 9–11.

Conclusion

In conclusion we have investigated the possible presence of local changes of "carbon-to-metal ratio" in the growth mechanism of carbon nanostructures grown from FePd-based and Fe_3C catalyst in conditions of steady state CVD and viscous-boundary-layer CVS experiments by pyrolysis of ferrocene and dichlorocyclooctadiene-palladium mixtures. We have demonstrated the observation of an unusual growth mechanism in which a direct transition from a CNOs morphology to a carbon fiber-like morphology is observed within the same carbon structure. This is found in conditions of low vapour flow-rates (in steady state flow) CVD and can be attributed to the concentration of Cl radicals in the pyrolysing vapour. The observed growth mechanism has been compared in detail with that reported for Fe_3C filled CNTs in previous reports on CVD of ferrocene/dichlorobenzene mixtures and with those reported in literature for other transition metal catalyst systems. In contrast, for experiments performed in the presence of a viscous boundary layer between the pyrolysed precursors and the used rough surface of the substrate a different result is found. Indeed radial CNTs structures filled with large quantities of $FePd_3$ and Fe_3C crystals are found as major product in this type of reaction. This latter result confirms the existence of the radial structure growth mechanism (involving the homogeneous nucleation of particles in a viscous boundary layer) also in presence of FePd-based catalyst species but in conditions of very low Cl concentration induced by the lower evaporation temperature. The morphological, cross-sectional and structural properties of the obtained carbon structures have been analyzed in detail by SEM, TEM, STEM, HRTEM, ED and X-ray diffraction.

Open Access Article. Published on 03 April 2017. Downloaded on 5/17/2026 12:24:15 AM.
This article is licensed under a Creative Commons Attribution-NonCommercial 3.0 Unported Licence.

Acknowledgements

We acknowledge Prof. Gong Min for his continuous support and the National Natural Science Foundation of China Grant No. 11404227.

Notes and references

1 S. Iijima, *Nature*, 1991, **354**, 56–58.
2 S. Iijima and T. Ichihashi, *Nature*, 1993, **363**, 603–605.
3 D. Ugarte, *Nature*, 1992, **359**, 707–709.
4 N. Sano, H. Wang, M. Chhowalla, I. Alexandrou and G. A. J. Amaratunga, *Nature*, 2001, **414**, 506–507.
5 L. Hultman, S. Stafstrom, Z. Czigany, J. Neidhardt, N. Hellgren, I. F. Brunell, K. Suenaga and C. Colliex, *Phys. Rev. Lett.*, 2001, **87**, 225503.
6 B. R. Elliott, J. J. Host, V. P. Dravida, M. H. Teng and J.-H. Hwang, *J. Mater. Res.*, 1997, **12**, 3328–3344.
7 N. Demoncy, O. Stephan, N. Brun, C. Colliex, A. Loiseau and H. Pascard, *Synth. Met.*, 1999, **103**, 2380–2383.
8 N. Demoncy, O. Stephan, N. Brun, C. Colliex, A. Loiseau and H. Pascard, *Eur. Phys. J. B*, 1998, **4**, 147–157.
9 H. Terrones, F. Lopez-Urias, E. Munoz-Sandoval, J. A. Rodriguez-Manzo, A. Zamudio, A. L. Elias and M. Terrones, *Solid State Sci.*, 2006, **8**, 303.
10 F. C. Dillon, A. Bajpai, A. Koos, S. Downes, Z. Aslam and N. Grobert, *Carbon*, 2012, **50**, 3674.
11 A. L. Danilyuk, A. L. Prudnikava, I. V. Komissarov, K. I. Yanushkevich, A. Derory, F. Le Normand, V. A. Labunov and S. L. Prischepa, *Carbon*, 2014, **68**, 337.
12 D. Golberg, M. Mitome, C. Muller, C. Tang, A. Leonhardt and Y. Bando, *Acta Mater.*, 2006, **54**, 2567.
13 S. Hampel, A. Leonhardt, D. Selbmann, K. Biedermann, D. Elefant, C. Muller, T. Gemming and B. Buchner, *Carbon*, 2006, **44**, 2316.
14 A. Leonhardt, M. Ritschel, R. Kozhuharova, A. Graffa, T. Muhl, R. Huhle, I. Monch, D. Elefant and C. M. Schneider, *Diamond Relat. Mater.*, 2003, **12**, 790.
15 C. Prados, P. Crespo, J. M. Gonzalez, A. Hernando, J. F. Marco, R. Gancedo, N. Grobert, M. Terrones, R. M. Walton and H. W. Kroto, *Phys. Rev. B: Condens. Matter Mater. Phys.*, 2002, **65**, 113405.
16 J. F. Marco, J. R. Gancedo, A. Hernando, P. Crespo, C. Prados, J. M. Gonzalez, N. Grobert, M. Terrones, D. R. M. Walton and H. W. Kroto, *Hyperfine Interact.*, 2002, **139**, 535.
17 F. S. Boi, G. Mountjoy and M. Baxendale, *Carbon*, 2013, **64**, 516.
18 Boi, R. M. Wilson, G. Mountjoy, I. Muhammad and M. Baxendale, *Faraday Discuss.*, 2014, **173**, 67–77.
19 J. Guo, J. Liu, M. Lan, Y. Hu, S. Wang, J. Wen, Y. He, F. Gao, X. Zhang, S. Zhang, G. Xiang, M. A. C. Willis and F. S. Boi, *RSC Adv.*, 2017, **7**, 4753.
20 F. S. Boi, J. Guo, G. Xiang, M. Lan, S. Wang, J. Wen, S. Zhang and Y. He, *RSC Adv.*, 2017, **7**, 845.
21 F. S. Boi, J. Guo, M. Lan, G. Xiang, S. Wang, J. Wen and S. Zhang, *Carbon*, 2015, **95**, 634–639.
22 F. S. Boi, J. Guo, M. Lan, G. Xiang, Y. He, S. Wang and H. Chen, *RSC Adv.*, 2016, **6**, 54189–54192.
23 J. Guo, Q. Ye, M. Lan, S. Wang, T. Yu, F. Gao, D. Hu, P. Wang, Y. He, F. S. Boi, S. Zhang and G. Xiang, *RSC Adv.*, 2016, **6**, 40676–40682.
24 R. S. Wagner and W. C. Ellis, *Appl. Phys. Lett.*, 1964, **4**(5), 89–90.
25 A. R. Harutyunyan, O. A. Kuznetsov, C. J. Brooks, E. Mora and G. Chen, *ACS Nano*, 2009, **3**, 379–385.
26 A. Moisala, A. G. Nasibulin and E. I. Kauppinen, *J. Phys.: Condens. Matter*, 2003, **15**, S3011–S3035.
27 M. Kumar and Y. Ando, *J. Nanosci. Nanotechnol.*, 2010, **10**, 3739–3758.
28 J. Guo, M. Lan, S. Wang, Y. He, S. Zhang, G. Xiang, *et al.*, *Phys. Chem. Chem. Phys.*, 2015, **17**, 18159–18166.
29 F. S. Boi, J. Guo, S. Wang, Y. He, G. Xiang, X. Zhang and M. Baxendale, *Chem. Commun.*, 2016, **52**, 4195–4198.
30 J. Guo, Y. He, S. Wang and F. S. Boi, *Carbon*, 2016, **102**, 372–382.
31 F. S. Boi, Y. Hu, S. Wang and Y. He, *RSC Adv.*, 2016, **6**, 69226.
32 W. Wang, K. Wang, R. Lv, W. J. Zhang, X. Kang, F. Chang, *et al.*, *Carbon*, 2007, **45**, 1105–1136.
33 R. Lv, F. Kang, W. Wang, J. G. J. Wei, K. Wang and D. Wu, *Carbon*, 2007, **45**, 1433–1438.
34 R. Lv, A. Cao, F. Kang, W. Wang, J. Wei and J. Gu, *J. Phys. Chem. C*, 2007, **111**, 11475.
35 R. Lv, S. Tsuge, X. Gui, K. Takai, F. Kang, T. Enoki, *et al.*, *Carbon*, 2009, **47**, 1141–1145.
36 X. Gui, K. Wang, W. Wang, J. Wei, X. Zhang, R. Lv, *et al.*, *Mater. Chem. Phys.*, 2009, **113**, 634–637.
37 R. Lv, F. Kang, J. Gu, X. Gui, J. Wei, K. Wang, *et al.*, *Appl. Phys. Lett.*, 2008, **93**, 223105.
38 H. Terrones, T. Hayashi, M. Munoz-Navia, M. Terrones, Y. A. Kim, N. Grobert, *et al.*, *Chem. Phys. Lett.*, 2001, **343**, 241–250.
39 D. Lupu, A. Radu Biris, I. Misan, A. Jianu, G. Holzhuter and E. Burkel, *Int. J. Hydrogen Energy*, 2004, **29**, 97–102.
40 Q. Ngo, A. M. Cassell, V. Radmilovic, J. Li, S. Krishnan, M. Meyyappan, *et al.*, *Carbon*, 2007, **45**, 424–428.
41 M. A. Atwatera, J. Phillipsa, S. K. Doornb, C. C. Luhrsa, Y. Fernandez, J. A. Menendezc and Z. C. Leseman, *Carbon*, 2009, **47**, 2269–2280.
42 Z. He, J. Luc Maurice, A. Gohier, C. S. Lee, D. Pribat, *et al.*, *Chem. Mater.*, 2011, **23**, 5379–5387.
43 J. Li, M. Zou, L. Chen, Z. Huang and L. Guan, *J. Mater. Chem. A*, 2014, **2**, 10634–10638.

 This journal is © The Royal Society of Chemistry 2017